10.1007/s12541-010-0007-2

Precision Control of a Piezo-Actuated Micro Telemanipulation System

Mohammad Zareinejad[1,#], Saeed Shiry Ghidary[2], Seyed Mehdi Rezaei[1] and Amir Abdullah[1]

1 School of 1 Department of Mechanical Engineering, Amirkabir University of Technology, Tehran 159163331, Iran
2 Department of Computer Engineering, Amirkabir University of Technology, Tehran 159163331, Iran
Corresponding Author / E-mail: mzare@aut.ac.ir, TEL: +98-21-66402044, FAX: +98-21-66402044

KEYWORDS: Micro Telemanipulation, Piezoelectric Actuator, Hysteresis, Sliding Mode, Impedance Control

Piezoelectric actuators are widely used in micro manipulation applications. However hysteresis nonlinearity limits accuracy of these actuators. This paper presents a novel approach for utilizing a piezoelectric nano-stage as slave manipulator of a teleoperation system. The Prandtl-Ishlinskii (PI) model is used to model actuator hysteresis in feedforward scheme to cancel out this nonlinearity. To deal with the influence of parametric uncertainties, unmodeled dynamics, and PI identification error a perturbation term is added to the slave model and apply a sliding mode based impedance control with perturbation estimation. The stability of the entire system is guaranteed by Llewellyn's absolute stability criterion. Performance of the proposed controllers is verified through experiments.

Manuscript received: February 3, 2009 / Accepted: October 26, 2009

1. Introduction

Telemanipulation defines the idea of a user interacting with and manipulating a remote environment and has led to applications ranging from space-based robotics to telesurgery.[1] Beside several applications of teleoperation systems there is a new application area which is called Macro-micro teleoperation. Man has restriction to sense or manipulate micro objects directly. Macro-micro teleoperation can enable human to manipulate tasks in micro world. Biomanipulation of cell for using in in-vitro fertilization (IVF) and other cell manipulation applications are among new Macro-micro teleoperation systems.[2] Teleoperation technology is also investigated for the development of emerging microsurgery systems.[3,4]

Micro assembly is another example of Macro-micro teleoperated systems. Assembly of micro and millimeter sized parts requires fine position resolution, below the micron range. As with the macro assembly, force reflection is essential. Teleoperated micro-assembly systems provide a solution to manual micro-assembly through overcoming scaling restriction and achieving high accuracies, while offering flexibility and an intuitive human-controlled working environment.[5] A teleoperated system for pushing and touching of micro particles using Atomic Force Microscope (AFM) is reported by Sitti et al.[6,7] It has been recognized that the presences of time delay is one of the most important barriers in teleoperation systems. This problem is mainly due to the distance separating the master from the slave site. It may also be due to lag effect of filters and motor drivers. To overcome this problem, many concepts such as Network Theory, Passivity and Scattering Theory have been used. The idea is to analyze mechanisms responsible for loss of stability and derive a time delay compensation scheme to guarantee stability.[19-22] The two-port network representation of teleoperation systems is used in several researches.[23,24] Llewellyn stability criterion for two-port networks is less conservative and applicable for linear systems.[23] Cho and Park[20] proposed a sliding mode based impedance control (SMBIC) for a linear system with uncertain parameters .The proposed robust impedance controller was designed based on a desired impedance model and the sliding-mode controller which has robustness to system uncertainty.

In this paper a piezo-actuated stage has been used as the slave manipulator of macro-micro teleoperation system. Piezoelectric actuator is an excellent choice as micro positioning actuator due to its high resolution, fast response and capability of producing high forces. Hysteresis effect of piezoelectric actuators which is revealed in their response to an applied electric field is the main setback in

precise position open-loop control. The Maximum error due to hysteresis can be as much as 10-15 % of the path covered if the actuators are run in an open-loop fashion.[8] Moreover unknown hysteresis characteristics cause difficulties in closed loop control design. The dynamic hysteresis relation between the applied voltage and the actuator displacement originates from a cascaded combination of a static hysteresis. This is between the applied voltage and the induced charge into the actuator. There is a linear electromechanical coupling between the induced charge and the excitation force. A linear dynamic relation between the excitation force and the actuator displacement is also present.[9] Although the effect of hysteresis could be bypassed with control of the induced charge, costly instrumentations are required for the measurement and amplification of the induced charge.[10,11] Voltage drive strategies are thus preferred despite their limiting hysteresis nonlinearity. Many methods have been proposed to compensate hysteresis on the actuation of piezoelectric actuators. Preisach[8,12] Maxwell,[13] second-order polynomial[14]are well known hysteresis models, however their approximation accuracy is limited and suffer from a complicated identification procedure. Kuhenen[15] proposed a modified Prandtl-Ishlinskii (PI) model for the hysteresis nonlinearity. This model has been extended for rate-dependent and load-dependent hysteresis.[16-18] PI model is less complex and its inverse can be computed analytically. In this study a modified PI model is applied and its inverse is utilized to cancel out the hysteresis effect. Accurate tracking of piezoelectric actuators with voltage steering strategy are extensively carried out in both feedforward and feedback control operations. Most feedforward controllers cascade an inverse hysteresis model in series with a piezoelectric actuator plant to cancel out the effect of nonlinearity and achieve a relatively linear response.[17,18] Cahyadi et al.[28] developed a 3-DOF macro-micro teleoperation system using piezoelectric actuator. The proposed controller for slave side did not consider uncertainty of model. Moreover, hysteresis effect after compensation (Figure 12)[28] depicts that remained nonlinearity is considerable. Bilateral telemanipulation systems attempt to provide force tracking in master side. (Figure 14)[28] depict proper position tracking and contact force of the slave. The paper did not provide any plot to explain force tracking. Furthermore the paper did not consider time delay which may destabilize the system in force reflecting teleoperation system.

In this paper, the nonlinear piezoelectric actuator is linearized using feedforward inverse hysteresis. The linearized uncertain model is then used to design the controller. The sliding-mode based impedance control with perturbation estimation scheme is used. With an impedance control for the master, a desired dynamic behavior between human operator and master device can be realized. Stability of the teleoperation system against time delay is performed using Llewellyn criterion and proper controller gains are adjusted to achieve stability and performance simultaneously. Llewellyn criterion which is applied for linear systems. However proposed approach provides a framework for using this stability criterion for nonlinear time delayed piezo-actuated telemanipulation systems.

2. Teleoperator Modeling

Fig. 1 shows the master slave system for a micro telemanipulation setup. To design an efficient controller for this system the dynamics equations of motion of the teleoperation system are first derived.

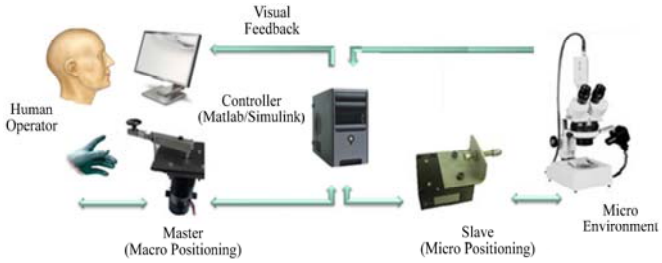

Fig. 1 Macro-micro Telemanipulation setup

2.1 Dynamic Modeling for the Master Robot

In this research the master is a 1 DOF manipulator which utilizes a DC servo motor. A load cell is installed on the shaft of the motor to measure the force exerted on the master. Dynamic model of the motor can be considered as follows:

$$j_m\ddot{\theta}_m(t)+b_m\dot{\theta}_m(t)+k_m\theta_m(t)=u_m(t)+L_mF_h(t) \tag{1}$$

where θ_m denote rotation angle, j_m, b_m and k_m are moment of inertia of the rotating system, damping and stiffness respectively. F_h is the force exerted by human operator and L_m is the effective length between the force and motor shaft. u_m is control signal that is applied to the master robot.

2.2 Dynamic Modeling for the Slave Robot

The slave manipulator consists of a 1-DOF stage actuated by a piezo stack actuator. Hysteresis effect of piezoelectric actuators which is revealed in their response to an applied electric field is the main drawback in precise positioning. Therefore, the development of a dynamic model which describes the hysteresis behavior is very important. This is for the improvement of the control performance of the piezo-positioning mechanism. In many investigations, a second-order linear dynamics has been utilized for describing the system dynamics. As shown in figure 2, this model combines mass-spring-damper ratio with a nonlinear hysteresis function appearing in the input excitation to the system.

The following equation defines the model:

$$m_s\ddot{x}_s(t)+b_s\dot{x}_s(t)+k_sx_s(t)=H_F(v(t)) \tag{2}$$

where $x_s(t)$ is the salve position, m_s, b_s and k_s are mass, viscous coefficient and stiffness respectively. $H_F(v(t))$ denotes the hysteretic relation between input voltage and excitation force. Piezoelectric actuators have very high stiffness, and consequently, possess very high natural frequency. In low-frequency operations, the effects of actuator damping and inertia could be safely neglected. Hence, the governing equation of motion is reduced to the following static hysteresis relation between the input voltage and actuator displacement:

$$x(t) = \frac{1}{k_s} H_F(v(t)) = H_x(v(t))$$
$$\{m_s \ddot{x}_s(t) \ll b_s \dot{x}_s(t) \ll k_s x_s(t)\} \quad (3)$$

Equation (3) facilitates the identification of the hysteresis function $H_x(v(t))$ between the input voltage and the excitation force.

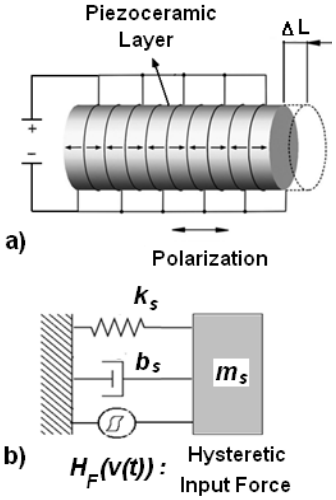

Fig. 2 (a) Piezoelectric stack actuator (b) Equivalent dynamic model

This is performed by first identifying the hysteresis map between the input voltage and the actuator displacement, $H_x(v(t))$. It is then, scaled up to k_s to obtain $H_F(v(t))$.

$$m_s \ddot{x}_s(t) + b_s \dot{x}_s(t) + k_s x_s(t) = k_s H_x(v(t)) \quad (4)$$

To consider the influence of parametric uncertainties, unmodeled dynamics, and identification error, a perturbation term $P(t)$ is added to the slave model. Thus the slave model (2) can be rewritten as the following:

$$\begin{aligned} & m_s \ddot{x}_s(t) + b_s \dot{x}_s(t) + k_s x_s(t) \\ & = H_F(v(t)) + P(t) \\ & = k_s H_x(v(t)) + P(t) \end{aligned} \quad (5)$$

To consider interaction with environment, the force F_e exerted by the environment is inserted into the model. Therefore dynamic model of the slave manipulator can be written as follows:

$$m_s \ddot{x}_s(t) + b_s \dot{x}_s(t) + k_s x_s(t) = k_s H_x(v(t)) + P(t) - F_e \quad (6)$$

3. Hysteresis Modeling

In this section hysteresis modeling using Prandtl-Ishlinskii (PI) is described. This model can approximate hysteresis loop accurately and its inverse could be obtained analytically. Therefore it facilitates the inverse feedforward control design.

3.1 Prandtl-Ishlinskii (PI)

There is a backlash operator in the PI hysteresis model (Fig. 3) that is defined by:

$$y(t) = H_r[x, y_0](t) = \max\{x(t) - r, \min\{x(t) + r, y(t - T)\}\} \quad (7)$$

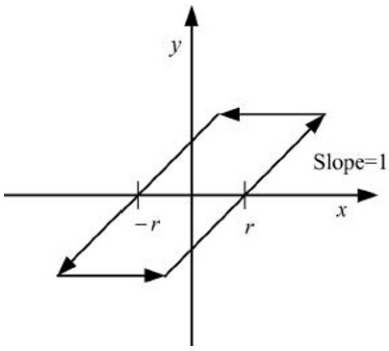

Fig. 3 The backlash operator

where x is the control input, y is the actuator response, r is the control input threshold value or the magnitude of the backlash and T is the sampling period. The initial consistency condition of (7) is given by

$$y(0) = \max\{x(0) - r, \min\{x(0) + r, y_0\}\} \quad (8)$$

where y_0 is usually but not necessarily initialized to 0. Multiplying the backlash operator H_r, by a weight value w_h, the generalized backlash operator is obtained:

$$y(t) = w_h H_r[x, y_0](t) \quad (9)$$

The weight w_h defines the gain of the backlash operator and may be viewed as the gear ratio in gear mechanical play analogy. Complex hysteresis nonlinearity can be modeled by a linear weighted superposition of many backlash operators with different threshold and weight values,

$$y(t) = \boldsymbol{W}_h^T \boldsymbol{H}_r[x, \boldsymbol{y_0}](t) \quad (10)$$

where

$$\boldsymbol{H}_r[x, \boldsymbol{y_0}](t) = [H_{r0}[x, y_{00}](t) \ldots H_m[x, y_{0n}](t)]^T \quad (11)$$

With the weight vector $\boldsymbol{W}_h^T = [w_{h0} \ldots w_{hn}]$, the threshold vector $\boldsymbol{r} = [r_0 \ldots r_n]^T$ where $0 = r_0 < \cdots < r_n$ and the initial state vector $\boldsymbol{y} = [y_0 \ldots y_n]^T$. The control input threshold values r_n are usually chosen to be of equal intervals between maximum and minimum of piezoelectric actuator displacement.

3.2 Modified PI Operator

The PI operator inherited the symmetry property of the backlash operator about the center point of the loop formed by the operator. The fact that most real actuator hysteretic loops are not synonymic weakens the model accuracy of the PI operator. To overcome this restrictive property, a saturation operator is combined in series with the hysteresis operator. A saturation operator is a weighted superposition of linear-stop or one-sided dead zone operators. A dead zone operator is a non-convex, non-symmetrical, and memory free nonlinear operator given by

$$S_d[x](t) = \begin{cases} \max\{x(t) - d, 0\} & d > 0 \\ x(t) & d = 0 \end{cases}$$
$$z(t) = \boldsymbol{w}_s^T \cdot \boldsymbol{S}_d[y](t) \quad (12)$$

Where y is the output of the hysteresis operator and, z is the

actuator response. $\boldsymbol{w}_s^T = [w_{s0} \dots w_{sm}]$, is the weight vector. $\boldsymbol{S}_d[y](t) = [S_{d0}[y](t) \dots S_{dm}[y](t)]$ with the threshold vector $\boldsymbol{d}^T = [d_0 \dots d_m]^T 0 = d_0 < \cdots < d_m$.

Thus the modified PI operator is defined as follows:

$$z(t) = H_x(t) = \boldsymbol{w}_s^T \cdot \boldsymbol{S}_d \lfloor \boldsymbol{w}_h^T \cdot \boldsymbol{H}_r[x, \boldsymbol{y}_0] \rfloor (t) \tag{13}$$

d_i is usually chosen to be equal intervals between maximum and minimum of hysteresis operator output.

3.3 Inverse model of PI

The inverse PI operator is given by

$$H_x^{-1}[x_d(t)] = \boldsymbol{w}_h'^T \boldsymbol{H}_{r'} \lfloor \boldsymbol{w}_s'^T \cdot \boldsymbol{S}_d[x_d], y_0' \rceil (t) \tag{14}$$

Cascading the inverse hysteresis model with the actual hysteresis model gives the identity mapping between the control input $x_d(t)$ and the actuator response $x(t)$.

$$x(t) = H_x[H_x^{-1}[x_d(t)]] \tag{15}$$

The inverse model parameters can be calculated analytically as follow

$$w_{h_0}' = 1/w_{h_0}; w_{s_0}' = 1/w_{s_0} \tag{16}$$

$$w_{h_i}' = \frac{-w_{h_i}}{\left(\Sigma_{j=0}^{i} w_{h_j}\right)\left(\Sigma_{j=0}^{i-1} w_{h_j}\right)}, \; i = 1 \dots n; \tag{17}$$

$$w_{s_i}' = \frac{-w_{s_i}}{\left(\Sigma_{j=0}^{i} w_{s_j}\right)\left(\Sigma_{j=0}^{i-1} w_{s_j}\right)}, \; i = 1 \dots n; \tag{18}$$

$$r_i' = \sum_{j=0}^{i} w_{h_j} (r_i - r_j), \; i = 0 \dots n; \tag{19}$$

$$d_i' = \sum_{j=0}^{i} w_{s_j} (d_i - d_j), \; i = 0 \dots m; \tag{20}$$

$$y_{0_i}' = \sum_{j=0}^{i} w_{h_j} y_{0_i} + \sum_{j=i+1}^{n} w_{h_j} y_{0_j}, \; i = 0 \dots n \tag{21}$$

After setting the threshold parameters r and d as described in the previous section, the weight parameters w_h and w_s are estimated by performing a least square fit of equation (13). Graphically, the inverse is the reflection of the resultant hysteresis loop about the 45° line.

3.4 Feedforward Hysteresis Compensation

The structure of inverse feedforward hysteresis compensation is shown in fig. 4. The key idea of an inverse feedforward controller is to cascade the inverse hysteresis operator H_x^{-1} with the actual hysteresis. This is represented by the hysteresis operator H_x to obtain an identity mapping between the desired actuator output $x_d(t)$ and actuator response $x(t)$. The inverse PI operator H_x^{-1} uses $x_d(t)$ as input and transforms it into a control input $v_{H_x^{-1}}(t)$ which produces $x(t)$ in the hysteretic system that closely tracks $x_d(t)$.

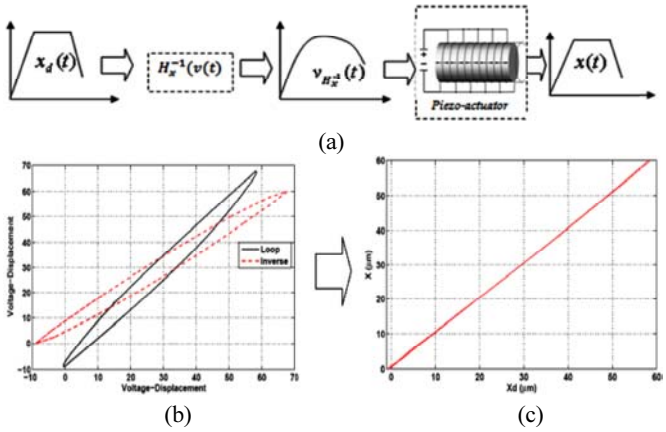

Fig. 4 (a) Inverse Feedforward hysteresis compensation (b) Hysteresis vs. inverse loop (c) x_d vs. x after compensation

3.5 Identification of the Hysteresis Model

In this section the method for identification of hysteresis function is described between the input voltage and the actuator displacement as defined by equation (13). Weighting parameters are identified using least-square optimization technique for error minimization. Static hysteresis is identified using quasi-static triangular input. Appropriate values for order of backlash operator n, saturation function m, and threshold vectors r, d are selected for proper approximation of hysteresis. The values for n and m can be set as 25 and 15 respectively.

Fig. 5 refers to the estimated hysteresis loop using PI model compared to the actual hysteresis of the piezo stage. Identification of PI parameters is performed for the measured actuator response subjected to $100v$ p-p sawtooth control input with frequency of 0.5 Hz.

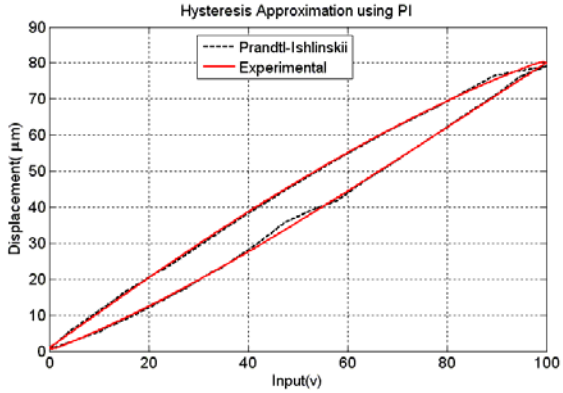

Fig. 5 Estimated hysteresis loop using PI vs. experimental result

4. Delayed Signals and Scaling Factors

When teleoperation is performed over a long distance, a time delay is incurred in the transmission of information from one side to the other side (figure 6). Another source of delay is the filtering effect of amplifiers and drivers that contribute a small amount of pure delay to the system. Other source of delay in the system can be the finite time required to execute the digital control loop.

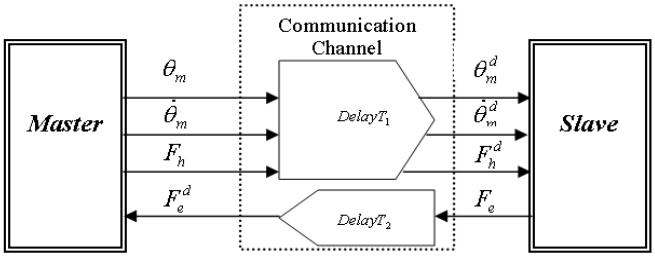

Fig. 6 Block diagram of the Teleoperator

To consider the time delay in the communication channel, the transmitted signals between master and slave can be represented as:

$$\begin{aligned} &\theta_m^d(t)=\theta_m(t-T_1) \quad \dot{\theta}_m^d(t)=\dot{\theta}_m(t-T_1) \quad F_h^d(t)=F_h(t-T_1) \\ &F_e^d(t)=F_e(t-T_2) \quad F_e^{dd}(t)=F_e(t-T_2-T_1) \end{aligned} \tag{22}$$

where $\theta_m^d(t)$, $\dot{\theta}_m^d(t)$ and $F_h^d(t)$ represent position, velocity and the force applied to the master by the operator. The signals transmitted from master to the slave face delay T_1. In the other hand the slave send the environment force F_e to the master with delay T_2. Thus the master receives it as $F_e^d(t)=F_e(t-T_2)$. If the master sends force signal $F_e^d(t)$ back to the slave, the arrival of the signal at the slave side will be delayed again by T_1 represented by $F_e^{dd}(t)=F_e(t-T_2-T_1)$.

These delayed signals are then scaled up or down by some factors depending on the teleoperation tasks, therefore:

$$x_s(t)=k_p\theta_m^d(t) \qquad \dot{x}_s(t)=k_p\dot{\theta}_m^d(t) \qquad F_h=k_fF_e^d(t) \tag{23}$$

where k_p and k_f are scaling factors for position/velocity and force, respectively.

5. Control Design

The main objective of impedance control is maintaining a desired dynamic relationship between robot position and contact force. This approach provides unique control architecture for both compliant and incompliant motions.

5.1 Impedance control for the master manipulator

An impedance controller is used for the master manipulator. The desired impedance for the master can be shown as:

$$\bar{J}_m\ddot{\theta}_m(t)+\bar{b}_m\dot{\theta}_m(t)+\bar{k}_m\theta_m(t)=L_m(F_h(t)-k_fF_e(t)) \tag{24}$$

where $\bar{J}_m$, $\bar{b}_m$ and $\bar{k}_m$ are the desired inertia, viscous damping coefficient, and stiffness, respectively. Right side of this equation reflects the scaled contact force between environment and slave manipulator. This force is exerted to the operator by desired impedance of master manipulator.

It is possible to replace the dynamics of the master (equation 1) with the desired dynamics (equation 24) using the following control law:

$$\begin{aligned} u_m(t)=&\left(b_m-\frac{j_m}{\bar{J}_m}\bar{b}_m\right)\dot{\theta}_m(t)+\left(\frac{j_m}{\bar{J}_m}-1\right)L_mF_h(t) \\ &-\frac{j_m}{\bar{J}_m}(k_fL_mF_e^d(t)+\bar{k}_m\theta_m(t)) \end{aligned} \tag{25}$$

5.2 Impedance Control for the Slave with Sliding Mode Based Perturbation Estimation

The desired dynamic for the slave manipulator is considered as follows:

$$\bar{m}_s\ddot{\tilde{x}}(t)+\bar{b}_s\dot{\tilde{x}}(t)+\bar{k}_s\tilde{x}(t)=-F_e \tag{26}$$

where $\bar{m}_s$, $\bar{b}_s$ and $\bar{k}_s$ are the desired mass, viscous damping coefficient, and stiffness of slave, respectively and $\tilde{x}(t)=x_s-k_p\theta_m^d$ is position error.

The control law of the slave controller is obtained by combining equations (26), (5):

$$\begin{aligned} u_s(t)=H_F^{-1}\{&-\frac{m_s}{\bar{m}_s}\left[b_s\dot{\tilde{x}}(t)+k_s\tilde{x}(t)+F_e(t)\right] \\ &+F_e(t)+k_sx_s(t)+b_s\dot{x}_s(t)+m_sk_p\ddot{\theta}_m^d-P_{est}\} \end{aligned} \tag{27}$$

To deal with the influence of parametric uncertainties, unmodeled dynamics and PI identification error, estimation of perturbation term P_{est} is added to the slave model. In next section the procedure for estimation of P_{est} is represented.

5.2.1 Perturbation Estimation

Elmali and Olgac have proposed a perturbation estimation scheme which is embedded in the traditional Sliding Mode Control (SMC) design.[24,25] The main advantage of this methodology is that a priori knowledge of the upper-bounds of perturbation is not required. The general class of nonlinear dynamics is considered as:

$$x^{(n)}=f(x)+\Delta f(x)+[B(x)+\Delta B(x)]u+d(t) \tag{28}$$

where $X_i=[x_i,\dot{x}_i,...,x_i^{(n-1)}]^T\varepsilon R^n$, $i=1,2,...,m$ is the state subvector and x_i, $i=1,2,...,m$ are m independent coordinates. $\Delta f(x)$ is perturbation of f, $\Delta B(x)$ is perturbation of control gain u and $d(t)$ is system disturbance vector. Perturbations and disturbance are gathered into a variable named perturbation vector:

$$\psi(X,t)_{actual}=\Delta f(x)+\Delta B(t)u+d(t)=x^{(n)}-f-Bu \tag{29}$$

If all the components in the dynamics show slower variations with respect to the loop closure (or sampling) speed, $\psi(X,t)$ can be estimated as:

$$\psi(X,t)_{estimated}=x_{calculated}^{(n)}-f-Bu(t-\delta) \tag{30}$$

where δ is the control interval or sampling time in the digital controller. In practice sampling time is selected high enough to ensure $u(t)=u(t-\delta)$. As shown in equation (30) the class of perturbation estimator is based on the simple intuition. This is if all the states are available, the perturbation of the plant can be effectively estimated using the nominal model and one step delayed input signals. Additionally, in the absence of measurements of $x^{(n)}$ an approximation is utilized as:

$$x^{(n)} = \frac{x^{(n-1)}(t) - x^{(n-1)}(t-\delta)}{\delta} \tag{31}$$

The errors in this estimation appear from two sources:

I) $x^{(n-1)}(t)$ measurements are often noisy. Therefore, their calculated time derivatives may manifest prohibitively large variations. The measurement noise of $x^{(n-1)}(t)$ should be filtered to a suitable level.

II) Regardless of the sampling speed the inequality $u(t) \neq u(t-\delta)$ holds.

It is important to note that the objective is not to reduce the estimation error to zero. No matter how large the actual perturbations are, the smaller the perturbation error, the better the performance. A modified version of system equation (5) could be written as

$$m_s \ddot{x}_s(t) + b_s \dot{x}_s(t) + k_s x_s(t) = H_F(v(t)) + P_{est}(t) - \tilde{P}(t) \tag{32}$$

where $\tilde{P}(t) = P_{est}(t) - P(t)$ is the error signal between the system perturbations and its estimation. Based on the perturbation estimation technique, an estimation of the perturbation function given in equation (5) is obtained as:

$$P_{est}(t) = m_s \ddot{x}_s(t) + b_s \dot{x}_s(t) + k_s x_s(t) - H_F(v(t-\delta)) \tag{33}$$

Substituting $H_F(v(t))$ by $k_s H_F(v(t))$ using (4) one can obtain

$$P_{est}(t) = m_s \ddot{x}_s(t) + b_s \dot{x}_s(t) + k_s x_s(t) - k_s H_x(v(t-\delta)) \tag{34}$$

5.2.2 Sliding mode based impedance control for slave robot using perturbation estimation

Sliding surface can be defined as following:

$$s(t) := \frac{1}{\bar{m}_s} \int_0^t I_e(t)dt \tag{35}$$

where I_e is the impedance error, that is:

$$I_e := \bar{m}_s \ddot{\tilde{x}}(t) + b_s \dot{\tilde{x}}(t) + \bar{k}_s \tilde{x}(t) - (-F_e(t)) \tag{36}$$

Theorem: For the system described by equation (6), if the control law is given by

$$\begin{aligned} v(t) = u_s(t) = H_F^{-1}\{-\frac{m_s}{\bar{m}_s}[b_s \dot{\tilde{x}}(t) + k_s \tilde{x}(t) + F_e(t)] \\ + F_e(t) + k_s x_s(t) + b_s \dot{x}_s(t) \\ + m_s k_p \ddot{\theta}_m^d - \gamma \operatorname{sgn}(S) - \lambda S - P_{est}\} \end{aligned} \tag{37}$$

where sgn(S) represent the signum function, γ and λ are the positive scalars, then asymptotically tracking of the system is guaranteed.

Proof: For analyzing the stability of the proposed control scheme, a Lyapunov function candidate is defined as:

$$V = \frac{S^2}{2} \tag{38}$$

The derivative of V with respect to time can be obtained as

$$\dot{V} = S\dot{S} \tag{39}$$

By substituting (36) in (3) one can obtain

$$\dot{V} = S\dot{S} = S[\dddot{\tilde{x}}(t) + \frac{\bar{b}_s}{\bar{m}_s} \ddot{\tilde{x}}(t) + \frac{1}{\bar{m}_s}(\bar{k}_s \dot{\tilde{x}}(t) + F_e(t))] \tag{40}$$

Utilizing (32) for substituting $\dddot{\tilde{x}}(t) = \dddot{x}_s - k_p \ddot{\theta}_m^d$ in (40), yields

$$\begin{aligned} \dot{V} = S[-k_p \ddot{\theta}_m^d + \frac{\bar{b}_s}{\bar{m}_s} \ddot{\tilde{x}}(t) + \frac{1}{\bar{m}_s}(\bar{k}_s \dot{\tilde{x}}(t) + F_e(t))] \\ + \frac{1}{m_s}[-b_s \ddot{x}_s - k_s \dot{x}_s + H_F(v(t)) + P_{est} - F_e - \tilde{P}(t)] \end{aligned} \tag{41}$$

Substituting $v(t)$ from (37) in (41) yields

$$\begin{aligned} \dot{V} = S[-k_p \ddot{\theta}_m^d + \frac{\bar{b}_s}{\bar{m}_s} \ddot{\tilde{x}}(t) + \frac{1}{\bar{m}_s}(\bar{k}_s \dot{\tilde{x}}(t) + F_e(t))] \\ + \frac{1}{m_s}[-b_s \ddot{x}_s - k_s \dot{x}_s + P_{est} - F_e - \tilde{P}(t)] \\ + \frac{1}{m_s} H_F\{H_F^{-1}\{-\frac{m_s}{\bar{m}_s}[b_s \ddot{\tilde{x}}(t) + k_s \dot{\tilde{x}}(t) + F_e(t)] + F_e(t) \\ + k_s x_s(t) + b_s \ddot{x}_s + m_s k_p \dddot{\theta}_m^d - \gamma \operatorname{sgn}(S) - \lambda(S) - P_{est}(t)\}\} \end{aligned} \tag{42}$$

(42) Can be rewritten as follows:

$$\begin{aligned} \dot{V} = S\dot{S} = S[-\frac{\lambda}{m_s} S - \frac{1}{m_s}\gamma \operatorname{sgn}(S) - \frac{\tilde{P}(t)}{m_s}] \\ = -\frac{\lambda}{m_s} S^2 - \frac{1}{m_s}\gamma|S| - \frac{\tilde{P}(t)}{m_s} S \end{aligned} \tag{43}$$

If the gain γ is selected such that condition $\gamma > |\tilde{P}(t)|$ is satisfied, (43) leads to

$$\dot{V} \leq -\frac{\lambda}{m_s} S^2 \leq 0 \tag{44}$$

Equation (44) depicts that time derivative of the positive definite Lyapunov function V is negative definite. Thus stability of the system is guaranteed. Essentially equation (44) states that the squared distance to the sliding surface, as measured by S^2 decreases along all system trajectories.

Chattering phenomena is the main problem of the sliding mode control and must be eliminated for the controller to perform properly. For this purpose controller discontinuity can be smoothed out by using a saturation function $sat\left(S/\varphi\right)$ instead of sgn(S). Where φ is boundary layer thickness. Therefore control law (37) can be rewritten as follows:

$$\begin{aligned} u_s(t) = H_F^{-1}\{-\frac{m_s}{\bar{m}_s}[b_s \dot{\tilde{x}}(t) + k_s \tilde{x}(t) + F_e(t)] \\ + F_e(t) + k_s x_s(t) + b_s \dot{x}_s(t) + m_s k_p \ddot{\theta}_m^d \\ - \gamma sat\left(S/\varphi\right) - \lambda S - P_{est}\} \end{aligned} \tag{45}$$

The acceleration term $\ddot{\theta}_m^d$ is replaced with lower-order using the delayed master so (45) leads to:

$$\begin{aligned} u_s(t) = H_F^{-1}\{-\frac{m_s}{\bar{m}_s}[b_s \dot{\tilde{x}}(t) + k_s \tilde{x}(t) + F_e(t)] + F_e(t) \\ + k_s x_s(t) + b_s \dot{x}_s(t) - \gamma sat\left(S/\varphi\right) - \lambda S - P_{est} \\ + k_p \frac{m_s}{\bar{J}_m}[-\bar{b}_m \dot{\theta}_m - \bar{k}_m \theta_m + L_f(F_h^d - k_f F_e^{dd})]\} \end{aligned} \tag{46}$$

6. Stability of the Entire System

Stability and Transparency are 2 major issues in teleoperation systems. They are defined as follows:[26]

I) Stability: Maintain stability of the closed-loop system irrespective of the behavior of the operator or the environment

II) Telepresence: Provide the human operator with a sense of Telepresence, with the latter regarded as transparency of the system between the environments and the operator.

There is a trade-off between the two above objectives and several control architectures try to improve transparency for stable teleoperation system.

Bilateral teleoperation is usually modeled as a two-port network. As electrical network analysis tools have been developed already for two-port networks, in this case, force and velocity of teleoperation system will be replaced with voltage and current in electrical two-port network respectively (Fig. 7)The inputs to teleoperation system are F_h^* and F_e^*. F_h^* is related to muscle force and F_e^* is usually assumed to be zero. Master, slave and communication channel are lumped into a two-port network called teleoperator. The two-port network can be represented by inputs, outputs and inter-relationships between them.

Definition1: A linear two-port system shown in Fig. 7 is said to be absolutely stable if there exists no set of passive terminating one-port impedance for which the system is unstable. If the network is not absolutely stable, it is potentially unstable. F_h (Contact force between master and operator) and $\dot{x}_s$ (velocity of slave side) are inputs. F_e (Contact force between slave and environment) and $\dot{\theta}_m$ (velocity of master side) are outputs. The linear relationship between inputs and outputs can be represented in hybrid matrix configuration. Using the Laplace notation, the hybrid matrix configuration is given as follows:

$$\begin{bmatrix} F_h \\ \dot{x}_s \end{bmatrix} = \begin{bmatrix} h_{11} & h_{12} \\ h_{21} & h_{22} \end{bmatrix} \begin{bmatrix} \dot{\theta}_m \\ -F_e \end{bmatrix} \tag{47}$$

The variables Z in Fig. 7 are impedance models which are defined as $Z = F/V$. It is clear that in order to analyze the stability of the whole teleoperation system, the teleoperator should be considered together with the environment and the human operator. If the human operator and the environment are assumed to be passive, the stability of the teleoperator can be analyzed independently.

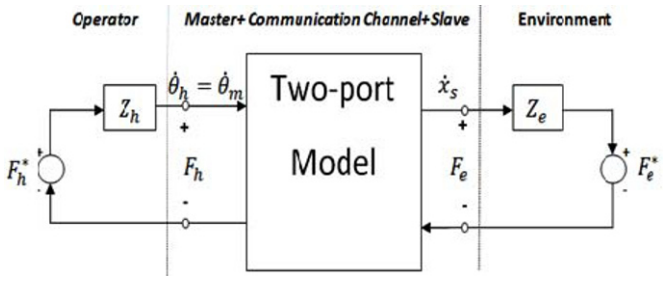

Fig. 7 A two-port teleoperation system

6.1 Llewellyn's criterion conditions:

For the two-port network represented by hybrid configuration matrix (equation 47), the necessary and sufficient Llewellyn's conditions for absolute stability in terms of the h-parameters are:

1. $h_{11}(s)$ and $h_{22}(s)$ have no poles in the right half plane
2. Any poles of $h_{11}(s)$ and $h_{22}(s)$ on the imaginary axis are simple with real and positive residues.
3. for all real values of $h_{11}(s)$ and $h_{22}(s)$ the inequalities (48) and (49) hold.

$$\mathrm{Re}[h_{11}] \geq 0,\ \mathrm{Re}[h_{22}] \geq 0 \tag{48}$$

$$\eta(\omega) = -\frac{\mathrm{Re}[h_{12}h_{21}]}{|h_{12}h_{21}|} + \frac{2\,\mathrm{Re}[h_{11}]\mathrm{Re}[h_{22}]}{|h_{12}h_{21}|} \geq 1 \tag{49}$$

These conditions represent Llewellyn's criterion for absolute stability. If any of the conditions is not satisfied, the network is potentially unstable. The condition (49) can also be rewritten as:[23]

$$\eta(\omega) = -\cos(\angle h_{12}h_{21}) - \frac{2\,\mathrm{Re}[h_{11}\,\mathrm{Re}\,h_{22}]}{|h_{12}h_{21}|} \geq 1 \tag{50}$$

This parameter η is called the network stability parameter. From (50) the value of the network stability parameter for a perfect transparent teleoperator can be calculated as $\eta = 1$ which means that the perfect transparent teleoperator is marginally absolutely stable. Absolute stability is applicable for linear systems.[27]

Values for $h_{ij}; i, j = 1,2$ are obtained from the following definitions and desired impedance models of master and slave robots according to the impedance models:

$$h_{11} = \frac{F_h(s)}{\dot{\theta}_m(s)} = \bar{J}_m(s) + \bar{b}_m + \frac{\bar{k}_m}{s} \tag{51}$$

$$h_{12} = \frac{F_h(s)}{F_e(s)} = -k_f e^{-T_2 s} \tag{52}$$

$$h_{21} = \frac{\dot{x}_s(s)}{\dot{\theta}_m(s)} = k_p e^{-T_1 s} \tag{53}$$

$$h_{22} = \frac{\dot{x}_s(s)}{F_e(s)} = \frac{s}{\bar{m}_s s^2 + \bar{b}_s s + \bar{k}_s} \tag{54}$$

The Llewellyn's criterion conditions 1 and 2 together with the first part of 3 are satisfied with positive impedance parameters. The

$$k_p k_f[\cos(T_1 + T_2)\omega - 1] + \frac{2\bar{b}_m \bar{b}_s \omega^2}{(\bar{k}_s - \bar{m}_s\omega^2)^2 + (\bar{b}_s\omega)^2} \geq 0 \tag{55}$$

Second part of condition 3 which is represented by equation (50) can be rewritten as:

Since $k_p k_f[\cos(T_1 + T_2)\omega - 1] \geq -2k_p k_f$

Therefore (55) is satisfied if

$$\frac{2\bar{b}_m \bar{b}_s \omega^2}{(\bar{k}_s - \bar{m}_s\omega^2)^2 + (\bar{b}_s\omega)^2} \geq k_p k_f \tag{56}$$

(56) Can be rewritten as following:

$$A\omega^4 + B\omega^2 + c \leq 0 \tag{57}$$

where:

$$A = k_p k_f \bar{m}_s^2 \tag{58}$$

$$B = k_p k_f (\bar{b}_s^2 - 2\bar{k}_s \bar{m}_s) - 2\bar{b}_m \bar{b}_s \tag{59}$$

$$C = \bar{k}_s^2 \tag{60}$$

In order to satisfy the inequality (57) two conditions should be met:

$$\text{i)} B < 0 \tag{61}$$

$$\text{ii)} B^2 - 4AC > 0 \tag{62}$$

In the next section impedance parameters are designed such that these conditions are satisfied.

7. Control Parameters

Parameters of controllers should be designed to maintain stability in all conditions while achieving a desired transparency. To meet the conditions given by equations (61) and (62) and achieving transparency, the desired impedance parameters for the master and slave robots are chosen as shown in Table 1. The values for controller gains and scaling factors of slave robot are shown in Table 2. k_p and k_f scaling factors, are selected according to the position range of master and slave robots. Position scaling factor k_p is designed such that with master rotation of 180°, piezo-stage moves 100μm.

Gains φ and γ must be selected experimentally to assure the robustness of the system against the ever present unmodeled dynamics and to moderate the chattering effect.

8. Experimental Results

8.1 System setup

In this section, the experimental results of the macro-micro teleoperation system are presented. The overall block diagram of this system including master, slave and proposed controllers is shown in Fig. 8. A Physik Instrument PZT-driven nanopositioning stage (PI 611.1s) with high resolution strain gage position sensor, is used for slave manipulator. The E500 Module includes E501 Piezo driver, E503 Strain gage amplifier which carry out experimental data. A rigid adjustable end effector is mounted on the stage. A load cell is used to measure environmental force (Fig. 9). A dSPACE data acquisition (DS1104) controller board is used as interface element between MATLAB Real time Workshop and the equipments. The controllers are developed in Simulink and implemented in real time using MATLAB and through dSPACE Control Desk software. The master manipulator consists of a DC servo motor which is equipped with a high resolution encoder. A load cell is installed on motor shaft to measure force exerted on the master (Fig. 10). An AX500 Digital Motor Controller is used for driving the DC servomotor. 2 load cell amplifiers are used to convert low voltage of load cells output to $0-10V$ range. A stereo

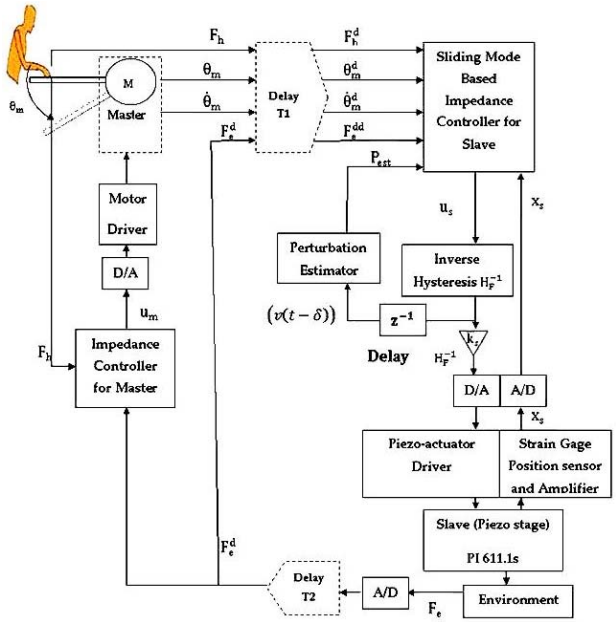

Fig. 8 The overall system block diagram

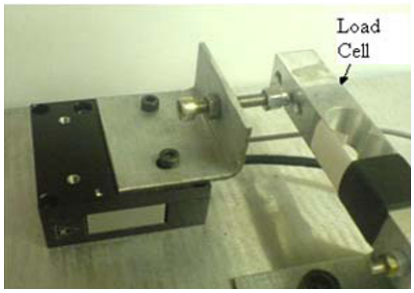

Fig. 9 Piezo stage as the slave manipulator

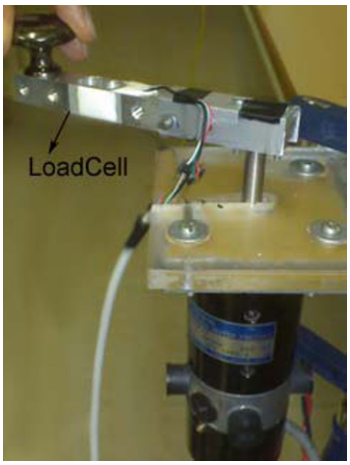

Fig. 10 The DC motor as the master manipulator

loop microscope equipped with a CCD camera is utilized to provide visual feedback.

For verification of proposed controllers human operator manipulates the master end-effector to generate a desired position trajectory. The external environment has a high stiffness that the slave end-effector cannot go into. Since its end is fixed on a rigid wall it behaves as a cantilever beam and interaction force causes displacement in the environment. The motion of the slave end-effector contains two stages as follows:

(I) Free motion when the slave end-effector does not contact with the loadcell.

(II) Interaction stage, when the slave end effector exerts force on the loadcell. At this stage, the end-effector exerts an interaction force on the external environment and also moves forward. Two experiments were performed. The first one without time delay and the second one with a time delay $T_1 + T_2 = 1.5s$.

As shown in Figs. 13, 14 position and force tracking could be performed in multi frequency reference signal and the proposed controller could provide proper maneuverability for operator.

In the arranged task the end-effector of the slave manipulator follows the master manipulator from the home position to the right wall until a contact occurs. After the contact the end-effector moves towards the front. It then keeps the master position for some seconds before returning to the home position. This task repeats several times.

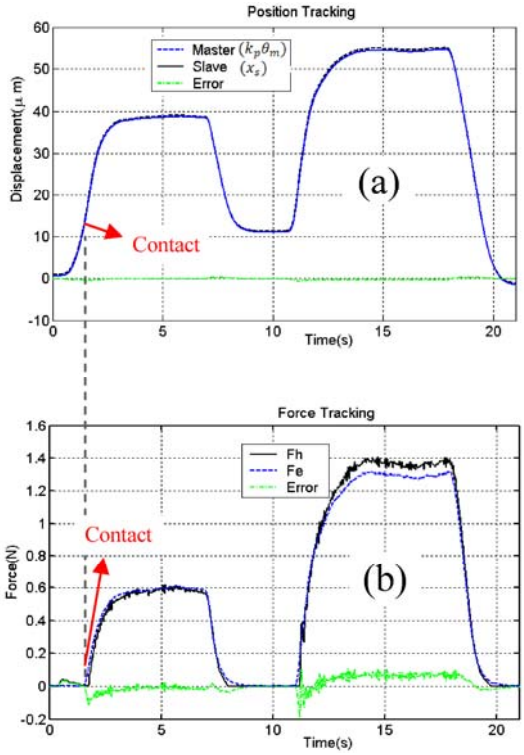

Fig. 11 (a) Master/slave position and (b) force signals without delay

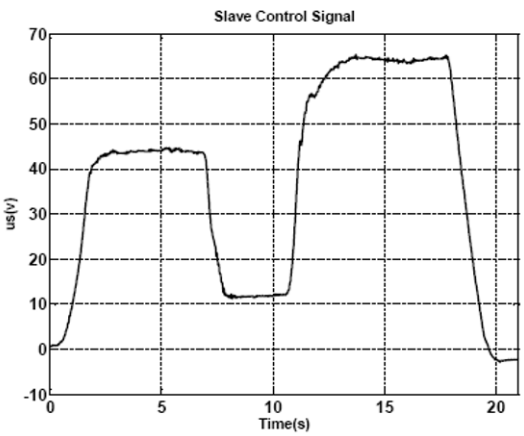

Fig. 12 Slave control signal using SMBIC

Figs. 11 and 12 show the experimental results for position and force tracking without time delay. The proposed scheme shows good tracking performance. In spite of the contact with environment, slave side can still track the master desired position (Fig. 11(a)) while force reflected back to the master side is increasing (Fig. 11(b)). The controllers are capable to achieve both position/force tracking. Fig. 12 depicts slave control signal which is chattering free. With proper parameter design the controller has been able to produce smooth control signal. Since operator tries to keep master in fixed position, hand chattering leads to noisy force signal. Experiments were also designed to show the maneuverability of the operator when using the proposed controller for arbitrary movement. Experimental results for position /force tracking under communication time delay are depicted in Figs. 15 and 16. T_1, T_2 was implemented using Simulink time delay. T_1, T_2 were set as $T_1 = 0.8s$ and $T_1 = 0.7s$ respectively. Filtering effect of amplifiers contribute a small amount of pure delay to the

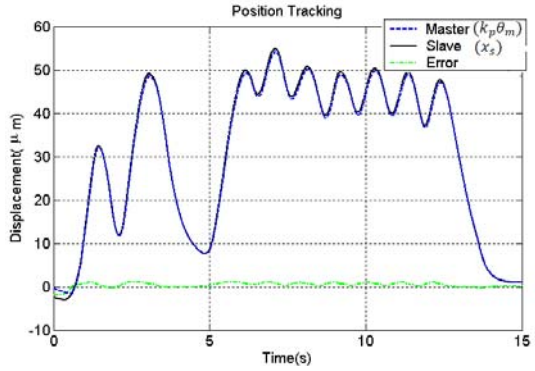

Fig. 13 Master/slave position signals without delay

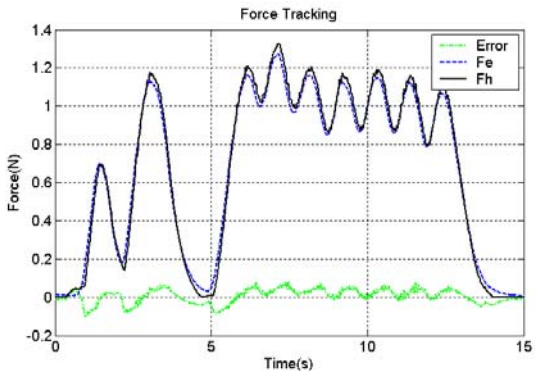

Fig. 14 Master/slave force signals without delay

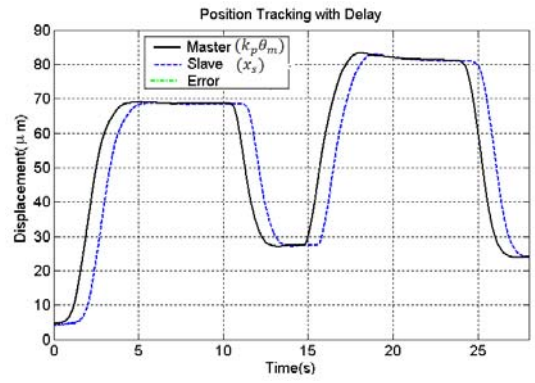

Fig. 15 Master/slave position signals with delay

system. A second source of delay in the system is the finite time required to execute the digital control loop. Therefore real delay would be larger than T_1, T_2. As shown in Figs. 15 and 16 the proposed control achieved good tracking performance. Figures 17 and 18 depict capability of proposed approach in tracking of scaled force ($Kf = 100$).

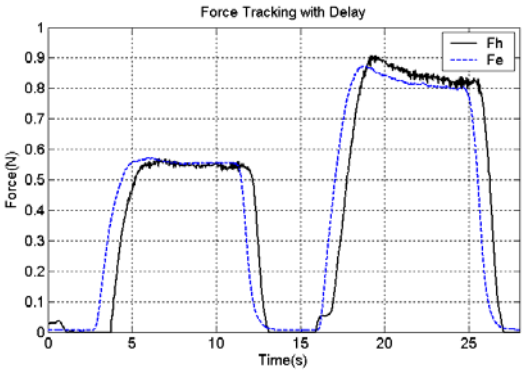

Fig. 16 Master/slave force signals with delay

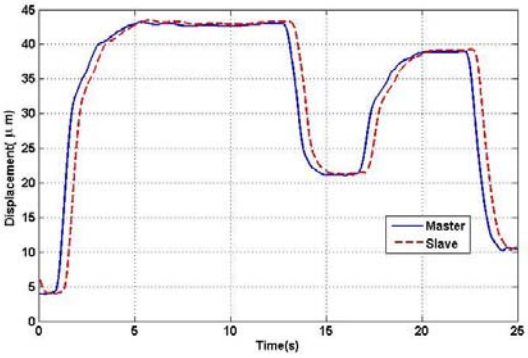

Fig. 17 Master/slave position signals with delay k_f=100

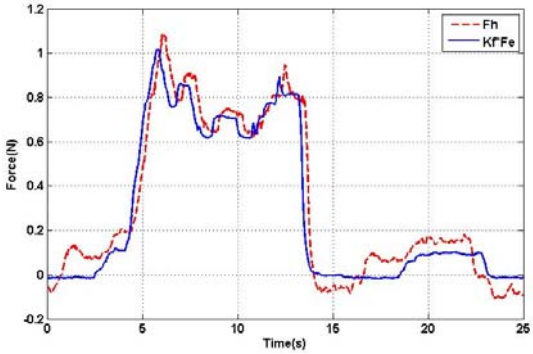

Fig. 18 Master/slave force signals with delay k_f=100

Remark 1: The amplitude of force in Figures 16, 14, 11(b) is not equal because in each experiment position of the end effector was different.

9. Conclusions

In this paper a macro-micro teleoperation was implemented using piezoelectric actuator as the slave manipulator. A nonlinear dynamic model for piezoelectric actuators was considered which combined a modified PI hysteresis operator with a second-order linear dynamic. An inverse model-based feedforward controller was then proposed and implemented to compensate hysteresis. To cope with remained nonlinearity and uncertainty of model a novel impedance control with sliding mode perturbation estimation was utilized.

An impedance controller for the master was implemented to achieve suitable force tracking. The proposed controllers make teleoperation robustly stable against uncertainties and bounded constant time delays. The nonlinear term of teleoperator, was compensated through the Feedforward inverse control. Thus stability of the linearized system is guaranteed by Llewellyn's absolute stability criterion which is applicable only for linear systems. Control parameters were tuned to satisfy stability conditions and good performance. The experimental results verifies the accurate position tracking in free motion and simultaneous position and force tracking in contact with low stiffness environment.

REFERENCES

1. Sheridan, T. B., "Telerobotics, Automation, and Human Supervisory Control," MIT Press, 1992.
2. Pillarisetti, A., Anjum, W., Friedman, G. and Brooks, A. D., "Force Feedback Interface for Cell Injection," Proceedings of the First Joint Eurohaptics Conference and Symposium on Haptic Interfaces for Virtual Environment and Teleoperator Systems, pp. 391- 400, 2005.
3. Gersem, D. G., "Kinaesthetic feedback and enhanced sensitivity in robotic endoscopic telesurgery," Ph.D. Dissertation, Department of Mechanical Engineering, Katholieke Universiteit Leuven, 2005.
4. Preusche, C., Ortmaier, T. and Hirzinger, G., "Teleoperation concepts in minimal invasive surgery," Control Engineering Practice, Vol. 10, Issue 11, pp. 1245-1250, 2002.
5. Sitti, M. and Hashimoto, H., "Macro to nano telemanipulation towards nanoelectromechanical systems," Journal of Robotics and Mechatronics, Vol. 12, No. 3, pp. 209-217, 2000.
6. Sitti, M. and Hashimoto, H., "Tele-Nanorobotics Using Atomic Force Microscope as a Robot and Sensor," Advanced Robotics Journal, Vol. 13, No. 4, pp. 417-436, 1999.
7. Onal, C. D., Pawashe, C. and Sitti, M., "A Scaled Bilateral Control System for Experimental 1-D Teleoperated Nanomanipulation Applications," Proceeding of the IEEE/RSJ International Conference on Intelligent Robots and Systems, pp. 483-488, 2007.
8. Ge, P. and Jouaneh, M., "Modeling hysteresis in piezoceramic actuators," Precision Engineering, Vol. 17, No. 3, pp. 211-221, 1995.

9. Bashash, S. and Jalili, N., "Robust Multiple Frequency Trajectory Tracking Control of Piezoelectrically Driven Micro/Nanopositioning Systems," IEEE Trans. Control Syst. Technology, Vol. 15, No. 5, pp. 867-878, 2007.

10. Newcomb, C. and Filnn, I., "Improving linearity of piezoelectric ceramic actuators," Electronic Letters, Vol. 18, No. 11, pp. 442-444, 1982.

11. Furutani, K., Urushibata, M. and Mohri, N., "Displacement control of piezoelectric element by feedback of induced charge," Nanotechnology, Vol. 9, No. 2, pp. 93-98, 1998.

12. Leang, K. K. and Devasia, S., "Design of hysteresis-compensating iterative learning control for piezo-positioners: Application to atomic force microscopes," Mechatronics, Vol. 16, No. 3, pp. 141-158, 2006.

13. Hu, H., Georgiou, H. M. S. and Ben-Mrad, R., "Enhancement of Tracking Ability in Piezoceramic Actuators," Mechatronics, Vol. 10, No. 2, pp. 230-239, 2005.

14. Kim, I., Kim, Y.-S. and Park, E.-C., "Sliding Mode Control of the Inchworm Displacement with Hysteresis Compensation," Int. J. Prec. Eng. Manuf., Vol. 10, No. 3, pp. 43-49, 2009.

15. Kuhnen, K. and Janocha, H., "Complex hysteresis modeling of a broad class of hysteretic nonlinearities," Proc. of the 8th Int. Conf. on New Achraiors, pp. 688-691, 2002.

16. Habibollahi, H. H., Rezaei, S. M., Ghidary, S. S., Zareinejad, M. and Seifabadi, R., "Hysteresis Compensation of Piezoelectric Actuator under dynamic load condition," Proceeding of the IEEE/RSJ International Conference on Intelligent Robots and Systems, pp. 1166-1171, 2007.

17. Lining, S., Changhai, R., Weibin, R., Liguo, C. and Minxiu, K., "Tracking control of piezoelectric actuator based on a new mathematical model," J. Micromechanics and Microengineering, Vol. 14, No. 11, pp. 1439-1444, 2004.

18. Ang, W. T., Garmon, F. A., Khosla, P. K. and Riviere, C. N., "Feedforward Controller with Inverse Rate-Dependent Model for Piezoelectric Actuators in Trajectory-Tracking Applications," Mechatronics, Vol. 12, No. 2, pp. 134-142, 2007.

19. Buttolo, P., Braathern, P. and Hannaford, B., "Sliding Control of Force Reflecting Teleoperation: Preliminary Studies," Presence, Vol. 3, No. 2, pp. 158-172, 1994.

20. Park, J. H. and Cho, H. C., "Sliding-mode controller for bilateral teleoperation with varying time delay," Proceedings of the IEEE/ASME International Conference on Advanced Intelligent Mechatronics, pp. 311-316, 1999.

21. Cho, H. C., Park, J. H., Kim, K. and Park, J.-O., "Sliding mode-based impedance controller for bilateral teleopertation under varying time-delay," Proceedings of the IEEE International Conference on Robotics and Automation, Vol. 1, pp. 1025-1030, 2001.

22. Niemeyer, G. and Slotine, J. J. E., "Towards Force-Reflecting Teleoperation over the Internet," Proc. Of IEEE Int. Conf. on Robotic and Automation, Vol. 3, pp. 1909-1915, 1998.

23. Haykin, S. S., "Active network theory," Addison-Wesley, 1970.

24. Elmali, H. and Olgac, N., "Sliding mode control with perturbation estimation (SMCPE): A new approach," Int. J. Control, Vol. 56, No. 4, pp. 923-941, 1992.

25. Elmali, H. and Olgac, N., "Implementation of sliding mode control with perturbation estimation (SMCPE)," IEEE Trans. Control Syst. Technol., Vol. 4, No. 1, pp. 79-85, 1996.

26. Hokayem, P. F. and Spong, M. W., "Bilateral Teleoperation: An Historical Survey," Automatica, Vol. 49, No. 12, pp. 2035-2057, 2006.

27. Hashtrudi-Zaad, K. and Salcudean, S. E., "Analysis of Control Architectures for Teleoperation Systems with Impedance/ Admittance Master and Slave Manipulators," International Journal of Robotics Research, Vol. 20, No. 6, pp. 419-445, 2001.

28. Cahyadi, A. I. and Yamamoto, Y., "Teleoperated 3-DOF micromanipulation system with force feedback capability: design and experiments," Industrial Robot, Vol. 35, No. 4, pp. 337-346, 2008.